

Nonequilibrium phase transition in surface growth

B. Chakrabarti and C. Dasgupta*

Centre for Condensed Matter Theory, Department of Physics, Indian Institute of Science, Bangalore 560012, INDIA
(December 2, 2024)

Conserved growth models that exhibit a nonlinear instability in which the height (depth) of isolated pillars (groves) grows in time are studied by numerical integration and stochastic simulation. When this instability is controlled by the introduction of an infinite series of higher-order nonlinear terms, these models exhibit, as a function of a control parameter, a non-equilibrium phase transition between a kinetically rough phase with self-affine scaling and a phase that exhibits mound formation, slope selection and power-law coarsening.

The nonequilibrium kinetics of the growth of films by the deposition of atoms on a substrate is of considerable experimental and theoretical interest [1,2]. While the process of kinetic roughening [1] leading to a self-affine interface profile has been extensively studied, there has been much recent interest [2–4] in a different mode of surface growth, involving the formation and coarsening of “mounds” (pyramid-like structures). The system is said to exhibit *slope selection* if the typical slope of the sides of the mounds remains constant during the coarsening process. The precise experimental conditions which determine whether the growth morphology would be kinetically rough or dominated by mounds are presently unclear. Traditionally, the formation of mounds has been attributed to the presence of the Ehrlich-Schwoebel (ES) step-edge barrier [5,6] which hinders the downward motion of atoms across the edge of a step. The destabilizing effect of the resulting “uphill” surface current is usually modeled in continuum growth equations [7,8] as a *linear instability* arising from a Laplacian of the height variable with a negative coefficient. If this uphill surface current is compensated by higher-order terms in the growth equation at a specific value of the slope, then that slope is selected by the system.

In this Letter, we show that mound formation and power-law coarsening with slope selection occurs in a class of well-known, conserved surface growth models as a result of a *nonlinear instability* which leads to a *dynamical phase transition* between kinetically rough and mounded morphologies. We consider the conserved, fourth-order, nonlinear growth equation proposed by Lai and DasSarma [9] and by Villain [10]:

$$\partial h'(\mathbf{r}, t') / \partial t' = -\nu \nabla^4 h' + \lambda' \nabla^2 |\nabla h'|^2 + \eta'(\mathbf{r}, t'), \quad (1)$$

where $h'(\mathbf{r}, t')$ represents the height variable at the point \mathbf{r} at time t' , ∇ and ∇^2 represent, respectively, the spatial derivative and Laplacian operators in d dimensions (the dimension of the substrate), and η' is a Gaussian, delta-correlated random noise. This equation is believed [2,9,10] to provide a correct description of the scaling behavior of kinetically rough surfaces of films grown by molecular beam epitaxy. Our results are based on numerical integration of this equation in one dimension,

using a simple Euler scheme [11]. Choosing appropriate units of height, length and time, and discretizing both space and time, Eq.(1) is written as [11]

$$h_i(t + \Delta t) - h_i(t) = \Delta t \tilde{\nabla}^2 [-\tilde{\nabla}^2 h_i(t) + \lambda |\tilde{\nabla} h_i(t)|^2] + \sqrt{\Delta t} \eta_i(t), \quad (2)$$

where $h_i(t)$ represents the dimensionless height variable at the lattice point i at dimensionless time t , $\tilde{\nabla}$ and $\tilde{\nabla}^2$ are lattice versions of the derivative and Laplacian operators, and $\eta_i(t)$ is a random variable with zero average and variance equal to unity. These equations, with an appropriate choice of the “time step” Δt , are used to numerically follow the time evolution of the interface. We have also studied an atomistic version [12] of Eq.(1) in which the height variables $\{h_i\}$ are integers. The time evolution of this model is defined by the following deposition rule. First, a site (say i) is chosen at random. Then the quantity

$$K_i(\{h_j\}) = -\tilde{\nabla}^2 h_i + \lambda |\tilde{\nabla} h_i|^2 \quad (3)$$

is calculated for the site i and all its nearest neighbors. Then, a particle is added to the site that has the smallest value of K among the site i and its nearest neighbors. In the case of a tie for the smallest value, the site i is chosen if it is involved in the tie; otherwise, one of the sites involved in the tie is chosen randomly. The number of deposited layers provides a measure of time in this model.

It was found earlier [11] that both these models exhibit a *nonlinear instability* in which isolated structures (pillars for $\lambda > 0$, grooves for $\lambda < 0$) grow rapidly and indefinitely if their height (depth) exceeds a critical value. This instability can be controlled [11] by replacing $|\tilde{\nabla} h_i|^2$ in Eqns.(2) and (3) by $f(|\tilde{\nabla} h_i|^2)$ where the nonlinear function $f(x) \equiv (1 - e^{-cx})/c$, $c > 0$ being a control parameter. This amounts to the introduction of an infinite series of higher-order nonlinear terms. We call the resulting models “model I” and “model II”, respectively. The time evolution of the height variables in model I is, thus, given by

$$h_i(t + \Delta t) - h_i(t) = \Delta t \tilde{\nabla}^2 [-\tilde{\nabla}^2 h_i(t) + \lambda (1 - e^{-c|\tilde{\nabla} h_i(t)|^2})/c] + \sqrt{\Delta t} \eta_i(t). \quad (4)$$

It was shown in Ref. [11] that if c is sufficiently large, then the instability is absent and both models exhibit the scaling behavior expected in kinetic roughening. In the present work, we show that as the value of c is decreased, these models exhibit a *first-order dynamical phase transition* to a mounded morphology at a critical value of c . The mounded phase exhibits power-law coarsening (interface width $W \sim t^{\beta'}$ with $\beta' \simeq 1/3$), while the slope of the triangular mounds remains constant. We present results for the phase diagram of these models in the (λ, c) plane and describe the results of a stability analysis that provides an understanding of the observed behavior. We also show that this mechanism of mound formation, slope selection and coarsening is *qualitatively* different from the conventional ES mechanism.

Our results are obtained for systems of different sizes ($40 \leq L \leq 1000$) with periodic boundary conditions. In most of our studies of model I, we used $\Delta t = 0.01$. We have checked that very similar results are obtained for smaller values of Δt . If the control parameter c is sufficiently large, then the nonlinear instability is completely suppressed and the models exhibit the usual dynamical scaling behavior with the expected [9] exponent values, $\beta \simeq 1/3$, the dynamical exponent $z \simeq 3$, and the exponent $\alpha = \beta z \simeq 1$. As the value of c is decreased with λ held constant, the instability makes its appearance: the height h_0 of an isolated pillar (for $\lambda > 0$) increases in time if $h_{min}(\lambda, c) < h_0 < h_{max}(\lambda, c)$. The value of h_{min} is nearly independent of c , while h_{max} increases as c is decreased. If c is sufficiently large, h_{max} is small and the instability does not affect the scaling behavior of global quantities such as W , although transient multiscaling at length scales shorter than the correlation length $\xi \sim t^{1/z}$ may be found [11]. As c is decreased further, h_{max} becomes large, and when isolated pillars with $h_0 > h_{min}$ are created at an initially flat interface through random fluctuations, the rapid growth of such pillars to height h_{max} leads to a sharp upward departure from the power-law scaling of W with time t . The time at which this departure occurs varies from run to run. Typical results obtained for model I with $\lambda = 4.0$ and $c = 0.02$ are shown in the inset of Fig.1.

The instability leads to the formation of a large number of pillars of height close to h_{max} . As the system evolves in time, the interface self-organizes to form triangular mounds of a fixed slope near these pillars. These mounds then coarsen in time, with large mounds growing larger at the expense of small ones. In this coarsening regime, a power-law growth of W in time is recovered. The slope of the sides of the triangular mounds remain constant during this process. Finally, the system reaches a steady state with one peak and one trough (this is due to the use of periodic boundary conditions) and remains in this state for longer times.

This behavior is illustrated in Fig.1 where the interface profiles in a typical run for a $L = 200$ system start-

ing from a flat state are shown at times $t = 200$ (before the onset of the instability), $t = 4000$ (after the onset of the instability, in the coarsening regime), and $t = 128000$ (in the final steady state). The inset shows the time-evolution of W in this run, as well as the results for W as a function of t , averaged over 40 runs for $L = 1000$ samples. The averaged data show a power-law *growth regime* with $\beta \simeq 1/3$ before the onset of the instability, and a second power-law *coarsening regime* with $W \sim t^{\beta'}$, $\beta' = 0.346 \pm 0.01$, at long times. The selection of a “magic slope” during the coarsening process is readily seen in the plots of Fig.1. More quantitatively, the distribution of the nearest-neighbor height differences $s_i \equiv |h_{i+1} - h_i|$ is found to exhibit a pronounced peak at the selected value of the slope, and the position of this peak does not change during the coarsening process.

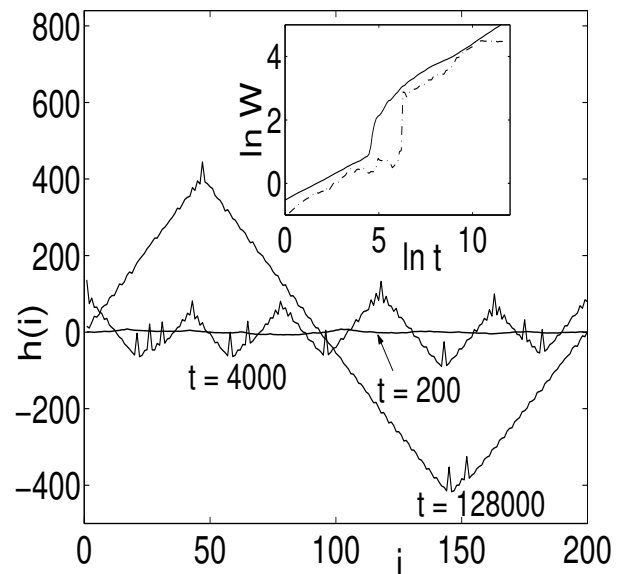


FIG. 1. The interface profile at three different times ($t = 200, 4000$, and 128000) in a run starting from a flat state for a $L = 200$ sample of model I with $\lambda=4.0$ and $c=0.02$. A double-log plot of the interface width W as a function of time t in this run is shown in the inset (dash-dotted line). The full line in the inset shows similar data averaged over 40 runs for $L = 1000$ samples.

While the saw-tooth-like surface profiles found for small c is qualitatively different from the self-affine morphology observed for large c , the interface width exhibits very similar power-law behavior in the two cases ($\beta \simeq \beta' \simeq 1/3$, and $\alpha' = 1 \simeq \alpha$). Thus, a measurement of the interface width would not distinguish between the two growth modes. A clear distinction between the two morphologies may be obtained from measurements of the average number of extrema of the height profile [13]. The steady-state profile in the mound-formation regime exhibits two extrema for *all* values of the system size L . In contrast, the number of extrema in the steady state

in the kinetic roughening regime increases with L as a power law [13] – we find that for values of c for which the system is kinetically rough, e.g. for $\lambda = 4.0$, $c = 0.05$, the average number of extrema in the steady state is proportional to L^δ with $\delta \simeq 0.83$. This observation allows us to define an “order parameter” that is zero in the large- c , kinetic roughening regime and finite in the small- c , mound-formation regime. Let σ_i be an Ising-like variable, equal to the sign of the slope of the interface at site i . An extremum in the height profile then corresponds to a “domain wall” in the configuration of the $\{\sigma_i\}$ variables. Defining

$$m = \frac{1}{L} \left| \sum_{j=1}^L \sigma_j e^{2\pi i j / L} \right|, \quad (5)$$

it is easy to see that in the mound-formation regime where there are two domain walls separated by $\sim L/2$ in the steady state, this quantity would be finite in the $L \rightarrow \infty$ limit. On the other hand, m would go to zero for large L in the kinetically rough regime because the number of domains in the steady-state profile would increase with L . We find numerically that $m \sim L^{-\gamma}$ with $\gamma \simeq 0.2$ for $\lambda = 4.0$, $c = 0.05$.

The behavior described above may be understood from a simple stability analysis. The profile near the top ($i = i_0$) of a mound may be approximated as $h_{i_0} = x_0 + x_1$, $h_{i_0 \pm j} = x_0 - (j-1)x_2$, where x_1 is the height of the pillar at the top of the mound and x_2 is the selected slope. The condition that this profile does not change under the dynamics of Eq.(4) with no noise leads to the following pair of non-linear equations for x_1 and x_2 :

$$\begin{aligned} 2x_1 - \lambda[1 - e^{-cx_2^2}]/c &= 0, \\ 3x_1 - x_2 - \lambda[1 - e^{-c(x_1+x_2)^2/4}]/c &= 0. \end{aligned} \quad (6)$$

These equations admit a non-trivial solution for sufficiently small c , and the resulting values of x_1 and x_2 are found to be quite close to the results obtained from numerical integration. A similar analysis for the profile near the bottom of a trough (this amounts to replacing x_2 by $-x_2$ in Eq.(6)) yields slightly different values for x_1 and x_2 . The full stable profile (a fixed point of the dynamics without noise) with one peak and one trough may be obtained numerically by calculating the values of h_i for which $g_i = 0$ for all i , where g_i is the term multiplying Δt in the right-hand side of Eq.(4). This calculation shows that the small mismatch between the values of x_2 near the top and the bottom is accommodated by creating a few ripples near the top. The numerically obtained fixed-point profile for a $L = 200$ system with $\lambda = 4.0$, $c = 0.02$ is shown in Fig.2, along with a typical steady-state profile for the same system. The two profiles are found to be nearly identical.

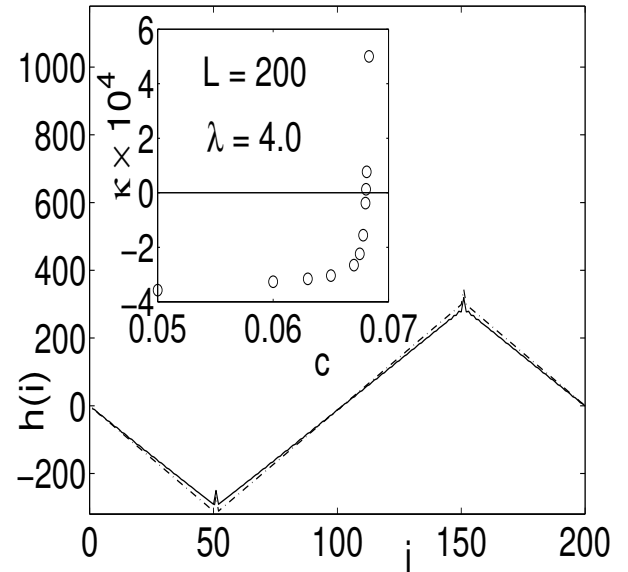


FIG. 2. Numerically obtained invariant height-profile for a $L = 200$ system with $\lambda = 4.0$, $c = 0.02$ (full line), and a snap shot of the same system in steady state (dash-dotted line). Inset: Zero-crossing of the largest eigenvalue κ of the stability matrix as a function of c ($\lambda = 4.0$, $L = 200$).

The local stability of the fixed-point profile may be determined from a calculation of the eigenvalues of the matrix $M_{ij} = \partial g_i / \partial h_j$ evaluated at the fixed point. We find that the largest eigenvalue of this matrix crosses zero at $c = c_1(\lambda)$ (see inset of Fig.(2)), signaling an instability of the mounded profile. The structure of Eq.(4) implies that $c_1(\lambda) \propto \lambda^2$. Thus, for $0 < c < c_1(\lambda)$, the dynamics of Eq.(4) without noise admits two locally stable invariant profiles: a trivial, flat profile with h_i the same for all i , and a non-trivial one with one mound and one trough. Depending on the initial state, the no-noise dynamics takes the system to one of these two fixed points. For example, an initial state with one pillar on a flat background is driven by the no-noise dynamics to the flat fixed point if the height of the pillar is smaller than a critical value, and to the mounded one otherwise.

In the presence of the noise, the perfectly flat fixed point transforms to the kinetically rough steady state, and the non-trivial fixed point evolves to the mounded steady state shown in Fig.1. A dynamical phase transition at $c = c_2(\lambda) < c_1(\lambda)$ separates these two kinds of steady states. To calculate $c_2(\lambda)$, we start a system at the mounded fixed point and follow its evolution according to Eq.(4) for a long time (typically $t = 10^4$) to check whether it reaches a kinetically rough steady state. By repeating this procedure many times, the probability, $P_1(\lambda, c)$, of a transition to a kinetically rough state is obtained. This probability P_1 for a fixed λ increases rapidly from 0 to 1 as c is increased beyond a critical value. Typical results for P_1 as a function of c for

$\lambda = 4.0$ are shown in the inset of Fig.3. The value of c at which $P_1 = 0.5$ provides an estimate of c_2 . Another estimate is obtained from a similar calculation of $P_2(\lambda, c)$, the probability that a flat initial state evolves to a mounded steady state at long times. As expected, P_2 increases sharply from 0 to 1 as c is decreased (see inset of Fig.3), and the value of c at which this probability is 0.5 is slightly lower than the value at which $P_1 = 0.5$. This difference reflects finite-time hysteresis effects. The value of c_2 is taken to be the average of these two estimates, and the difference between the two estimates provides a measure of the uncertainty in the determination of c_2 . The phase boundary obtained this way is shown in Fig.3, along with the results for $c_1(\lambda)$.

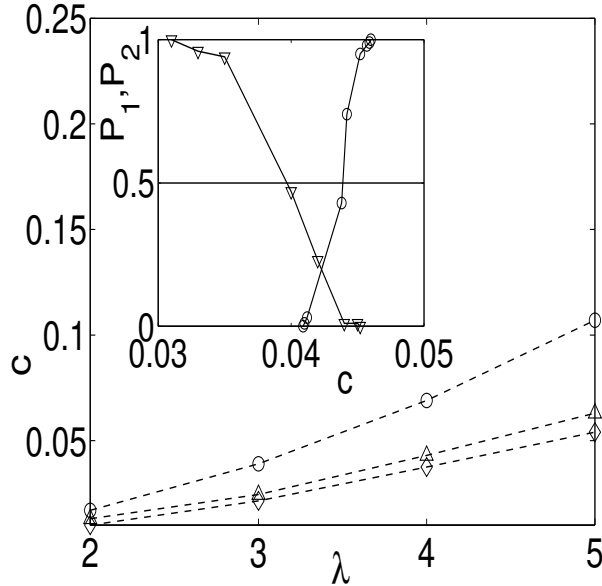


FIG. 3. Critical values of the control parameter c as functions of λ : c_1 of model I (circles), c_2 of model I (triangles), and c_2 of model II (diamonds). Inset: The probabilities P_1 (inverted triangles) and P_2 (circles) defined in text, as functions of c for model I with $\lambda = 4.0$, $L = 200$.

Our numerical results for model II are very similar. Height profiles of a $L = 200$ sample with $\lambda = 2.0$, $c = 0.005$ at three times (before the onset of the instability, during coarsening, and at the steady state) are shown in Fig.4. The inset shows the time-evolution of the interface width in this run and also the average over 40 runs for $L = 1000$ samples.

The qualitative behavior found here is very similar to that in canonical first-order transitions in equilibrium systems. In a time-dependent Ginzburg-Landau description [14] of the dynamics of a system exhibiting a first-order transition, the no-noise dynamics exhibits two locally stable fixed points (corresponding to the uniformly ordered and disordered states) in a range of temperatures near the transition temperature. In the presence of noise, the system selects one of the phases corresponding to

these two fixed points, except at the transition temperature where both phases coexist. The local stability of the mean-field ordered and disordered states leads to finite-time hysteresis effects near the transition temperature. The behavior we find is very similar, with the rough and the mounded states corresponding to the disordered and the ordered states of equilibrium systems and c playing the role of the temperature. In analogy with the behavior of equilibrium systems, we find hysteresis and coexistence of rough and mounded morphologies near $c = c_2$.

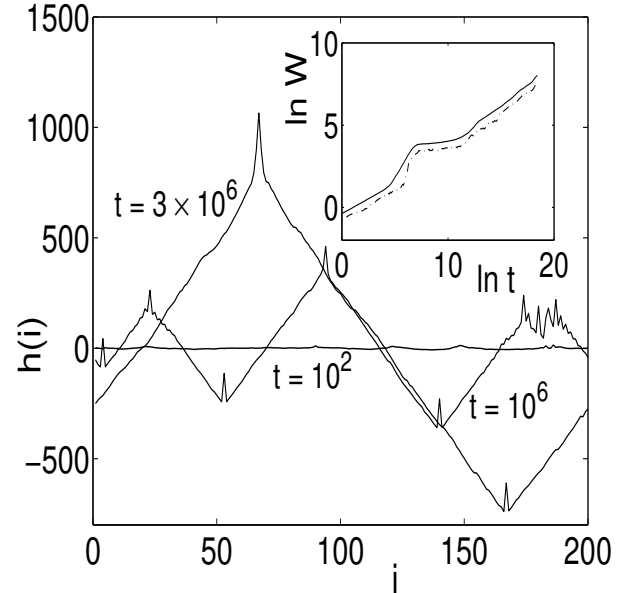


FIG. 4. The interface profile at three times ($t = 10^2$, 10^5 , and 3.10^6) in a run starting from a flat state for a $L = 200$ sample of model II with $\lambda = 2.0$ and $c = 0.005$. A double-log plot of the interface width W as a function of time t in this run is shown in the inset (dash-dotted line). The full line in the inset shows similar data averaged over 40 runs for $L = 1000$ samples.

In summary, we have shown that a nonlinear instability in a well-known class of surface growth models leads to mound formation and power-law coarsening with slope selection via a dynamical phase transition. It is important to emphasize that this mechanism of mound formation is very different from the conventional ES mechanism. The ES instability is usually modeled [7,8] as a *linear* one arising from a $\nabla^2 h$ term with a negative coefficient. Such a term is clearly absent in our models. Consequently, a flat interface is *locally stable* in our models. Since the non-equilibrium surface current in our models vanishes for *all* values of a constant slope, the slope selection we find is a true example of nonlinear pattern formation. In contrast, slope selection occurs in ES-type models because the surface current vanishes only at a *specific value* of the slope. Finally, we note that the behavior found in our models does not depend crucially on the form of the function $f(x)$: any monotonic

function that is linear for small x and saturates for large x is expected to produce similar results. In particular, we have found very similar behavior using a physically motivated [8] form, $f(x) = x/(1 + cx)$, for the control function.

We thank S. DasSarma for helpful discussions and SERC, IISc for computational facilities.

* Also at the Condensed Matter Theory Unit, JNCASR, Bangalore 560064, India.

- [1] A.-L. Barabasi and H. E. Stanley, *Fractal Concepts in Surface Growth* (Cambridge University Press, Cambridge, 1995).
- [2] J. Krug, Adv. Phys. **46**, 139 (1997).
- [3] J. Krim and G. Palasantzas, Int. J. Mod. Phys. **B9**, 599 (1997).
- [4] G. Lengel, R. J. Phaneuf, E. D. Williams, S. Das Sarma, W. Beard, and F. G. Johnson, Phys. Rev. B **60**, R8469 (1999), and references therein.
- [5] G. Ehrlich and F. G. Hudda, J. Chem. Phys. **44**, 1039 (1996).
- [6] R. L. Schwoebel, J. Appl. Phys. **40**, 614 (1969).
- [7] M. Siegert and M. Plischke, Phys. Rev. Lett. **73**, 1517 (1994).
- [8] P. Politi and J. Villain, Phys. Rev. B **54**, 5114 (1996).
- [9] Z. W. Lai and S. Das Sarma, Phys. Rev. Lett. **66**, 2348 (1991).
- [10] J. Villain, J. Phys. I (France) **1**, 19 (1991).
- [11] C. Dasgupta, J. M. Kim, M. Dutta, and S. Das Sarma, Phys. Rev E **55**, 2335 (1997).
- [12] J. M. Kim and S. Das Sarma, Phys. Rev. Lett. **72**, 2903 (1994).
- [13] Z. Toroczkai, G. Korniss, S. Das Sarma, and R. K. P. Zia, Phys. Rev. E. **62**, 276 (2000).
- [14] S.-K. Ma, *Modern Theory of Critical Phenomena* (Benjamin, Reading, 1976).